Engineering Failure Analysis 113 (2020) 104544

Contents lists available at ScienceDirect

Engineering Failure Analysis

journal homepage: www.elsevier.com/locate/engfailanal

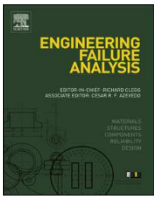

Failure analysis of fretting fracture in frame rails of heavy duty trucks – Case study

Vinay N. Rao*, Jeffrey W. Eischen

North Carolina State University, Raleigh 27606, NC, USA

ARTICLE INFO

Keywords:
Fretting fatigue
Crack growth simulation
Fracture
Complete vehicle
Finite element analysis

ABSTRACT

This paper analyzed fatigue fracture of a frame rail during accelerated endurance test of a heavy duty truck. This fracture was noted in an area of high shear stresses where contact and fretting fatigue was suspected. A cross section through the fracture initiation site showed areas of surface contact wear in the microstructure. Fretting wear resulted in crack initiation and propagated to form a through crack under reverse bending fatigue crack growth mechanism. A combination of crack growth simulation tool (FRANC3D) and finite element analysis solver (MSC NASTRAN) was used and automated to handle multiple crack growth iterations. The simulation results obtained showed good correlation to failure crack path and cycles to failure. These simulation results were also used to understand the root cause of failure, identify critical parameters causing failure and recommend design modifications to prevent fretting fatigue in frame of heavy duty trucks. A modified design using the proposed simulation methodology was identified and was shown to provide improved frame durability.

1. Introduction

Fretting fatigue initiation and damage occurs in contacting components when they are subjected to oscillating normal loads and sliding movements at the same time. At the contact interface surface wear and high contact stress conditions are created under cyclic loading. Fretting is mainly dependent on contact conditions such as surface finish, contact type (edge, spherical, cylindrical, etc.) and coefficient of friction [1–4]. These factors in turn affect normal force distribution, relative displacement and contact stress magnitudes. The damage obtained due to fretting fatigue can result in fretting wear (permanent material loss), crack nucleation and crack growth leading to catastrophic failure.

Fretting fatigue of heavy duty truck components is very common since all vehicle parts (brackets, cross members and load carrying rails) are fastened (bolts, rivets, welds) together and are subjected to random vibrations, bending and shear loads. A complete vehicle has large a number of connected parts which transfer stiffness through surface contact with adjacent parts. This large number of contact mechanisms and its interdependencies occurring in a full vehicle body makes it difficult to identify and prevent fretting fatigue. The fretting wear driven crack propagation and failure may occur in many applications such as bearings shafts, bolted and riveted connections, steel cables, steam and gas turbines.

Many investigators have predicted fretting fatigue life using a combination of finite element analysis and crack growth simulation tool [5–11]. Hojjati et al. [5], Jin et al. [10] and Proudhon et al. [11] performed cylinder/plane fretting wear simulation using simple 2D finite element analysis coupled with a LEFM code. Their study characterized fretting fatigue behavior of simple cylinder on flat

* Corresponding author.
E-mail address: vnrao@ncsu.edu (V.N. Rao).

https://doi.org/10.1016/j.engfailanal.2020.104544
Received 20 April 2016; Received in revised form 8 April 2018; Accepted 13 April 2020
Available online 14 April 2020
1350-6307/

contact configuration under mixed mode conditions.

Carter et al. [6] , Barlow et al. [7] and Ferjaoui et al. [9] showed crack growth simulation using component level 3D finite element analysis and fracture analysis simulation tool for typical fretting problems (dovetail joints in turbine blades, bolted joints) under mode-I, mode-II and mixed mode conditions. They studied effect of different axial stresses and contact forces on fretting induced crack propagation trajectories. Rajasekaran et al. [8] used a coarse finite element model and developed a semi-analytical model to estimate surface tractions and subsurface stress fields in dovetail blade root of an aircraft gas turbine. They simulated fretting fatigue using dovetail approximated as a 'flat and round' contact under half-plane assumptions.

Unlike the controlled fretting fatigue tests conducted using a test rig [12–15] this work studied fretting on frame rail during full vehicle endurance test. In this work a conventional strain fatigue approach was used to identify the crack initiation cycles for a low cycle fatigue of frame section under high shear stress with a reinforcement plate. The driving force for fretting is the relative slip amplitudes between the frame and reinforcement plate under varying track loads acting on the vehicle. The test track induced random vibrations and frame articulations are highly nonlinear and create high magnitude shear stresses in bolted and riveted components. This paper presents the results of varying reinforcement geometry and plate thickness to identify optimal stiffness distribution and to reduce fretting induced shear stresses. The effect of contact geometry on fretting stress distribution was investigated in this paper to identify the optimal design solution.

2. Experimental procedure

Endurance test procedures are developed based on customer vehicle usage activities, field service loads measured and known critical failure loads. Testing involves driving the vehicle over different road conditions. Each of these road conditions replicate customer usage of a vehicle in real conditions. Loads applied on vehicle include in-phase and out-of-phase high speed events (belgian blocks), high frequency random inputs, high magnitude transient loads (corner bumps), frequency sweeps (corrugations), quasi-static articulation (chassis twister) and axle roll events, low and high speed maneuvering (turning) events, braking and high gradient topographical events. A full vehicle endurance test typically reduces validation time by combining individual testing of multiple components into a single test. Depending on the operational class to which the vehicle is used different testing events are selected. A full description of test events cannot be provided due to confidentiality agreement.

Endurance testing is generally done at different speeds and at different gross vehicle weight rating (GVWR). These test events provide dynamic interactions between different vehicle modules and subsystems, enable dynamic interference and clearance check. The test vehicle is generally instrumented with strain gages, load transducers and accelerometers to measure vehicle response during testing. The data measured (strain, displacement and acceleration history) are generally used to validate new designs and improve numerical model development. The damage obtained for each cycle of loading is normally scaled to target loading cycles of a particular test event. The total damage obtained for all the repeats of test events in endurance test provides an estimate for the number of miles driven prior to failure of a particular component measured. The damage observed on different vehicle parts obtained after endurance testing is generally studied to see if design modifications can be implemented to make the parts more resistant to the damage and wear. Fig. 1, provides schematic representation for some of the endurance test events used for full vehicle validation,

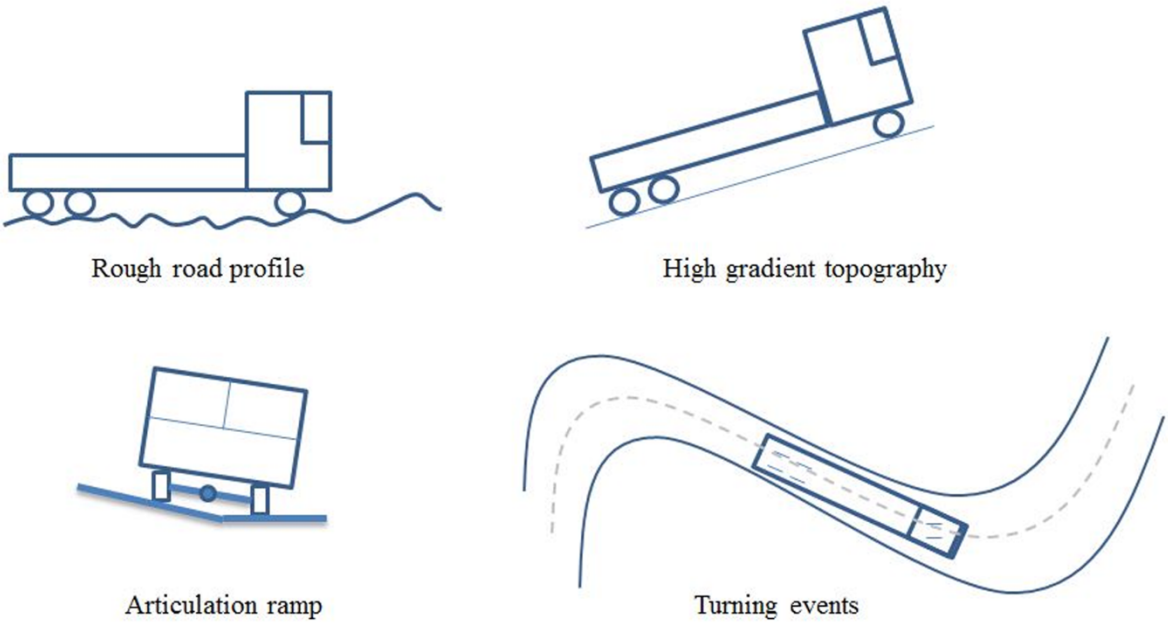

Fig. 1. Full vehicle endurance test events.

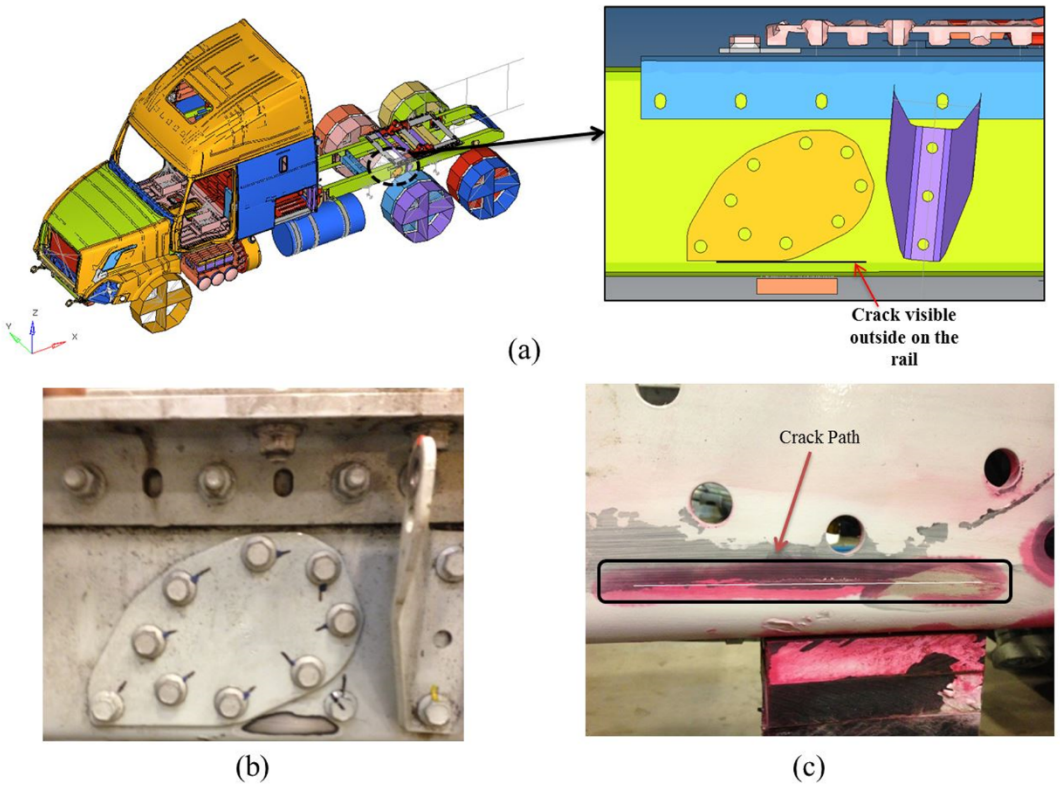

Fig. 2. (a) Location of frame crack shown in a full vehicle model (b) Frame outer reinforcement plate and frame crack path along lower edge contact (c) Crack path visible on frame after removing the outer reinforcement plate.

3. Experimental results

A full vehicle endurance test was conducted as part of project release for multiple chassis components. The aim of full vehicle test is to validate multiple components and study system behavior under varied frequencies and loads. The test was stopped at midway of endurance cycle (240 cycles out of 500 cycles) after a clearly visible frame crack was noticed near front drive axle torque rod connection. A visual inspection of frame crack (without disassembling chassis components) did not reveal fretting zone and was considered to be a fatigue failure. However, upon investigation it was found that fretting wear was found in the area of crack growth indicating that perhaps fretting was also associated with the initiation of the fatigue crack. Furthermore fractographic analysis indicated a shear lip towards the outer surface of the frame section indicating fatigue crack growth was from the inner surface to the outer surface of the frame section. Since the crack growth was from the inner surface to the outer surface and since the inner surface was predominately in cyclic compression, this indicated that crack initiation was likely initiated as a result of fretting.

Fig. 2 shows the layout of the vehicle and the area of failure noticed on the vehicle. The observed crack was near the front drive axle torque rod connection to frame and the crack path was observed to be longitudinal and coinciding with the edge of frame outer reinforcement bracket, as shown in Fig. 2(a). In Fig. 2(b) and Fig. 2(c) the extent of crack path on frame rail is highlighted. The crack path on frame rail was coincident with edge of outer and inner frame reinforcement plate.

3.1. Visual and SEM observation

A closer inspection of cracked section revealed that the shear lip was towards the outer surface of frame as shown in Fig. 3(a). This indicated the crack initiation and growth from the inner surface of the frame section. The optical micrograph of the cross sectioned fracture showed an area of contact wear deformation near the crack initiation site as shown in Fig. 3(b). The contact wear removed coating layers and exposed the base metal to corrosive environment. In Fig. 3(b), arrow shows the direction of fatigue crack propagation in reversed bending. It can be seen there was wear driven crack initiation on one end and a shear lip on the other side. A magnified view of the fracture initiation site (box) is shown in Fig. 4(b).

The fretting fatigue of frame rail was considered to be a result of edge contact shear stresses developed between the inner reinforcement plate and frame rail of the vehicle. The rear suspension components of a heavy duty truck are subjected to high magnitude oscillatory loads, resulting in fretting between contacting surfaces of torque bracket reinforcement plate and frame inner surface. A visual failure inspection revealed wear and corrosive degradation of material on the frame inner surface and just below the central bolt hole used on the torque rod bracket. This wear coincided with the edge contact of frame inner reinforcement, thus

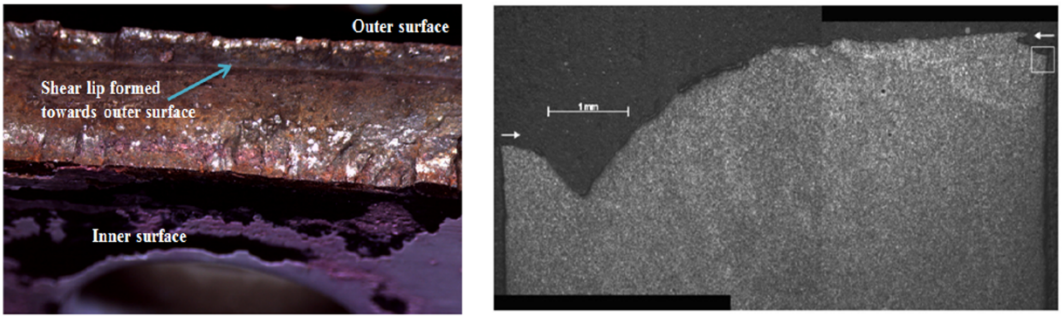

Fig. 3. (a) Section of the crack zone shows shear lip towards outer surface indicating crack origin on inner surface of frame (b) Optical micrograph of the cross sectioned frame fracture.

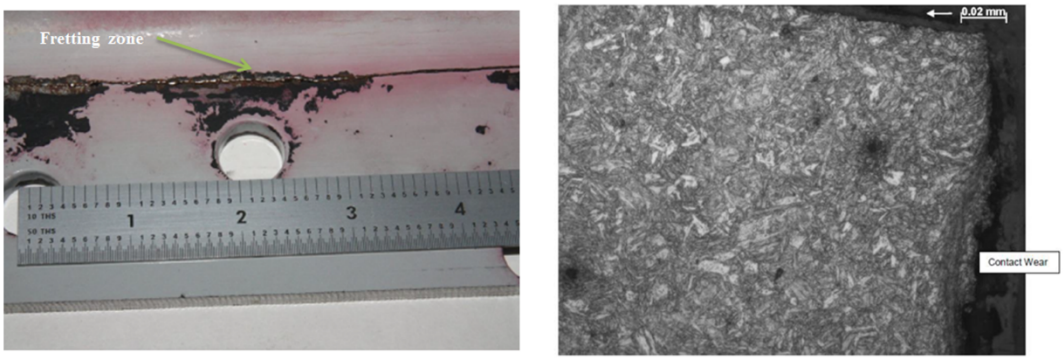

Fig. 4. (a) Fretting induced wear seen below central bolt hole on frame (b) Magnified view of the fracture initiation site, contact wear visible along initiation site.

indicating the presence of fretting. This location on the frame was not expected to see high tensile stresses and any crack initiation in this area would be due to high shear stress obtained during sliding movement between frame and inner reinforcement.

Fig. 4(a) shows the location of fretting zone below the lower bolt hole and along the contact edge of inner reinforcement plate. In Fig. 4(b) contact wear due to fretting is visible on the surface. The arrow indicates the direction of fatigue crack propagation. Optical micrograph in Fig. 3(b) showed shear lip, suggesting the crack initiation from inside section of frame and growth through the thickness under reverse bending fatigue.

The heavy duty truck frame used in this investigation was fabricated from 7 mm thick quenched and tempered wrought carbon steel having 120ksi minimum tensile strength. The tensile properties and hardness of frame material used in test are shown in Table 1. The base metal hardness of the frame section was found to be 32 HRC, which was in the expected range for quenched and tempered low carbon / manganese / boron steel. The effect of residual stress was not considered in this paper. The material (MET1123) used for frame rails in this vehicle was plasma cut and heat treated later to reduce the area of heat affected zone [16].

4. Simulation results

The main focus of the simulation methodology used in this study is to describe fretting failure in frame rail with friction included to account for both alternating principal and shear stresses in all modal transient loads. The simulation result obtained in the absence of friction has been studied and described in dissertation work of Rao [23]. It was observed [23] that the absence of contact stresses would predict damage in a different location and would lead to wrong root cause of failure conclusion.

The first step used in this study for developing a subsystem crack growth simulation model involves identifying the nodes which define the boundary of the sub-domain from the full vehicle model. Next, all the force/displacements obtained along the interface /

Table 1
Frame tensile properties and hardness.

Tensile Strength (ksi / MPa)	Yield Strength 0.2% Offset (ksi / MPa)	Elongation (%)	Hardness (HRC)
147 / 1013	138 / 951	16	32

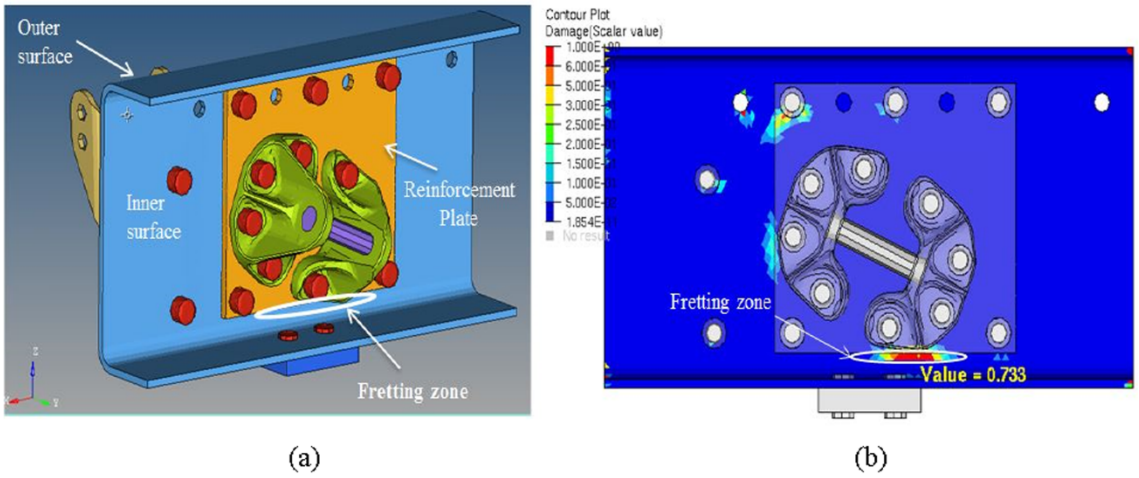

Fig. 5. (a) 3D solid subsystem model used for representing the area of durability concern (b) Fatigue result indicating high damage along fretting zone.

boundary nodes were extracted for complete transient road loads. A peak valley reduction methodology was applied to identify high magnitude loads. The subsystem model was then run through fatigue analysis by cycling the critical loads identified through the full vehicle modal transient analysis.

In Fig. 5(a) the reduced model includes the frame section where fracture occurred, reinforcement brackets as used in the test vehicle and associated bolts as per the specifications. This three-dimensional finite element model (NASTRAN SOL400) considers large displacement nonlinear behavior, nonlinear surface contact definitions and assembly loads (pre-tensioned bolts). Fig. 5(b) shows high damage distribution in the area of fretting zone as observed in physical test. The damage calculation was done using Coffin-Manson strain life model (Eq. (1)) and mean stress correction was considered using Morrow model. Simulation was performed for one cycle of each track event and a linear summation of fatigue damage was done for multiple repeats of different track events using Miner's rule. Damage calculated is the inverse of "cycles to failure" for the load applied.

The fatigue result obtained was based on Coffin-Manson strain life model,

$$\frac{\Delta\epsilon}{2} = \frac{\sigma_f^{'}}{E}(2N_f)^b + \epsilon_f^{'}\,(2N_f)^c \tag{1}$$

The Morrow model was used for mean stress correction and the elastic part of the Strain-Life curve is modified by the mean stress 'σ_m' as,

$$\epsilon_e = \frac{(\sigma_f^{'} - \sigma_m)}{E}(2N_f)^b \tag{2}$$

where N_f is the number of cycles to failure, σ'_f is the fatigue strength coefficient, b is the fatigue strength exponent and E is the modulus of elasticity. The effective strain used for fatigue calculation equals the von-Mises equivalent strain as,

$$\epsilon_{eff} = \sqrt{\frac{2(\epsilon_{xx}^2 + \epsilon_{yy}^2 + \epsilon_{zz}^2 + 2\epsilon_{xy}^2 + 2\epsilon_{xz}^2 + 2\epsilon_{yz}^2)}{3}} \tag{3}$$

Strain amplitude,

$$\epsilon_a = \frac{(\sigma_f^{'} - \sigma_m)}{E}(2N_f)^{2b} + \epsilon_f^{'}\,(2N_f)^c \tag{4}$$

The material parameters for the strain life equation were consistent with the frame material used in test. It can be observed that the predicted damage distribution is concentrated at the contact edge between frame and reinforcement plate and distributed along the fracture zone. The reinforcement plate and torque rod bracket were clamped using Grade 8 M14 bolts. An installation torque of 140 Nm or a clamp load of 50 kN was specified for each bolt in the model. The coefficient of friction (COF) considered for analysis was assumed to be 0.5 for varying test track profile and driving conditions. This was generally considered for analysis by taking an average between the extremes (COF = 0.9 for dry condition and COF = 0.1 for wet condition/smooth tire). A No further study was done with different coefficient of friction values. maximum fatigue damage of "0.733" or 73% of frame fatigue life being consumed was obtained from fatigue analysis of the subsystem model using the peak loads identified from full vehicle modal transient analysis (Fig. 5(b)). The simulated total damage obtained is based on multiple repeats of different test track events in a particular operational class of the vehicle. A design safety factor of 2 was generally targeted for frame section and hence a simulation prediction of fatigue damage above "0.5" was considered unacceptable and potential failure during physical test was expected.

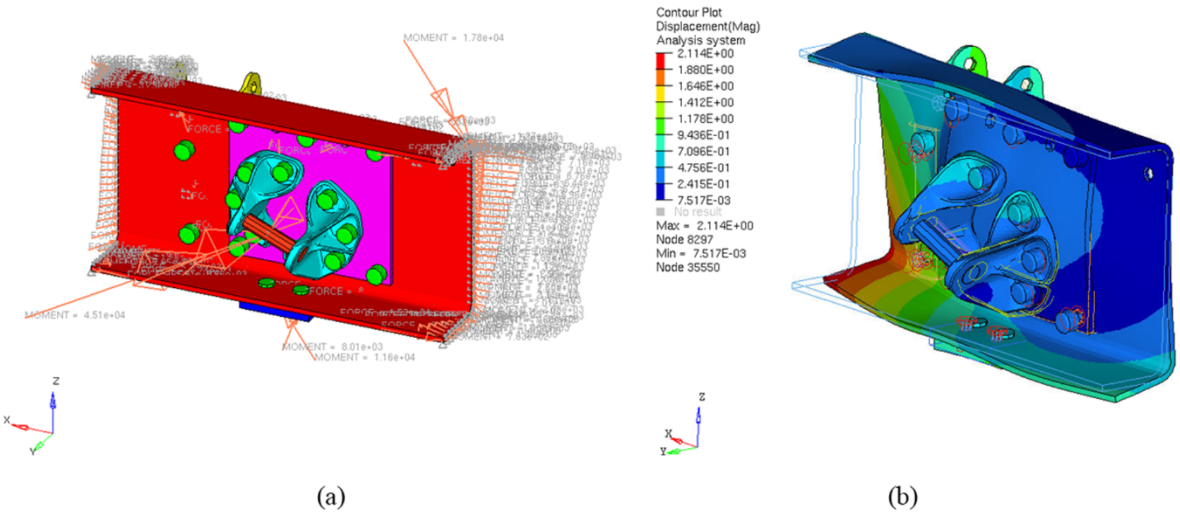

Fig. 6. (a) Multi-axial loading on frame section (b) Displacement plot under multi-axial loads.

Fig. 6(a) above shows the interface forces applied on the subsystem model used for fatigue and crack growth simulation. The loads were obtained from modal transient analysis of a full vehicle model for multi-axial test track excitations. Fig. 6(b) shows displacement plot indicating frame twist and bend mode obtained under multi-axial loading. Simulation of peak loads on the subsystem model showed high shear stress along the area of fretting concern. The crack growth was chosen to be for constant amplitude fatigue type and the crack kink angle was determined using strain energy release rate method. Paris law was used for fatigue growth rate model and the coefficients for Paris law were obtained from the frame supplier [16] (coefficient 'C' = 2e-8, exponent 'm' = 2.23 and threshold 'ΔK_{th}' = 316.2 MPa√mm). The Paris law is given as,

$$\frac{da}{dN} = C\Delta K^m \tag{5}$$

Where, a is the crack length, N is the number of load cycles, $\frac{da}{dN}$ provides crack growth rate, C and m are material constants, and ΔK is the range of the stress intensity factor, i.e., the difference between the stress intensity factor at maximum and minimum loading.

Stress intensity factors (SIF) were computed using Interaction Integral (M − Integral) method and include effects of crack face contact and crack pressure. A reverse bending fatigue was observed for certain frame twist loads and any crack initiation due to fretting was predicted to grow through the thickness under Mode I conditions.

Fig. 7(a) shows crack insertion (circled area) in the area of high shear stress of the local FRANC3D model and Fig. 7(b) shows semi-elliptical crack front (a = b = 0.5 mm with 'a' being horizontal width along contact surface and 'b' through the thickness) as obtained in FRANC3D visualization.

The crack growth simulation was performed using a considerable fine mesh size (element size approaching ~ 0.1 mm near crack tip) of the subsystem model. This paper did not include any mesh dependence study. This subsystem model with inserted crack is analyzed using finite element solver NASTRAN SOL400. The nodal displacements along the crack front is extracted and will be used

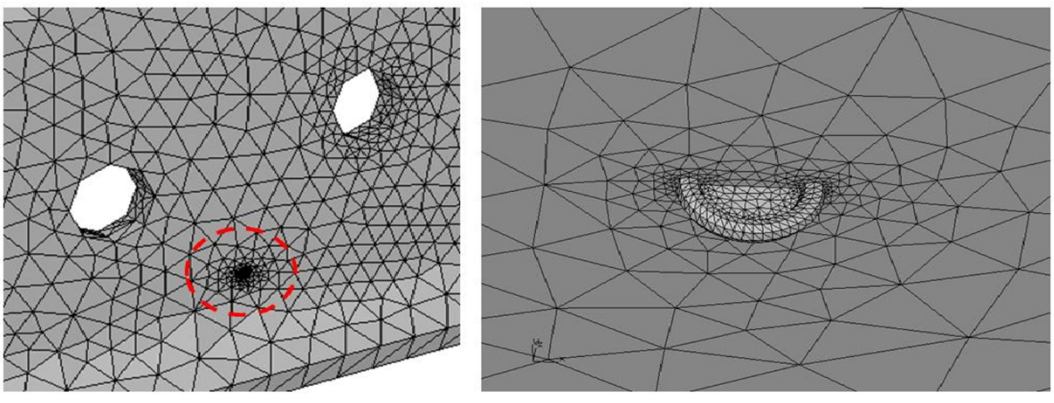

Fig. 7. (a) FRANC3D local model with semi-elliptical surface crack inserted (b) Semi-elliptical crack as visible through the thickness in FRANC3D.

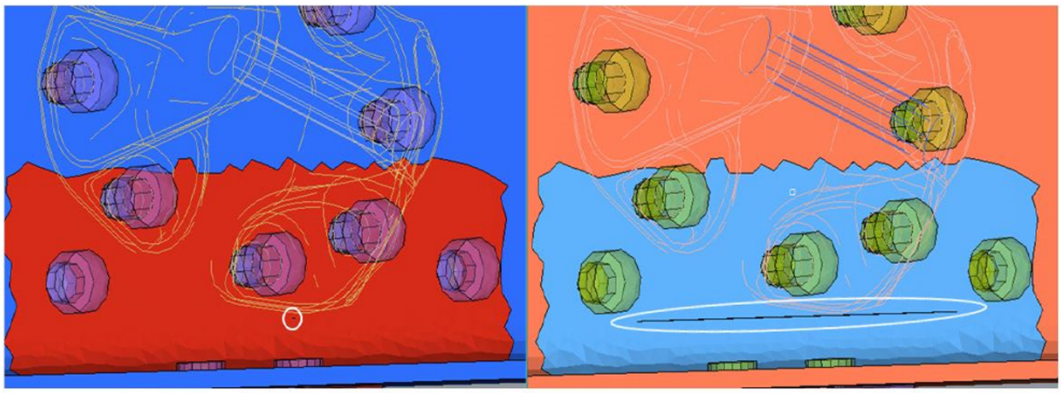

Fig. 8. (a) A small surface semi-elliptical crack initiated in the area of high fretting damage (b) Crack growth obtained after 6 steps of simulation run.

in FRANC3D to compute stress intensity factors to identify the next crack tip orientation and crack growth magnitude. The crack growth increments were determined by fatigue crack growth rate model (Paris law) for every step. The crack initiation cycles was obtained as (1/0.733 = 1.36 Endurance life = 1.36*500) 682 cycles. The crack growth cycles were considered to be very small, the crack once initiated due to fretting was expected to grow into large cracks under high stress amplitudes of track loads. Fig. 8(a) shows the initial crack and Fig. 8(b) shows the crack growth after 6 steps. The longitudinal axis of the initiated cracks was oriented parallel to the longitudinal axis of the frame. The axis of the initiated fatigue cracks are aligned with the maximum alternating shear stress directions. The crack once initiated and allowed to grow under fatigue loads extends along the outer surface and also through the thickness forming a complete through (the thickness) crack. This crack growth simulation result was observed to be along the contact edge between frame and inner reinforcement bracket and similar to the test result as shown in Fig. 2.

In Fig. 9, the crack growth history is shown where each step requires computing stress intensity factors (SIF) after growing the

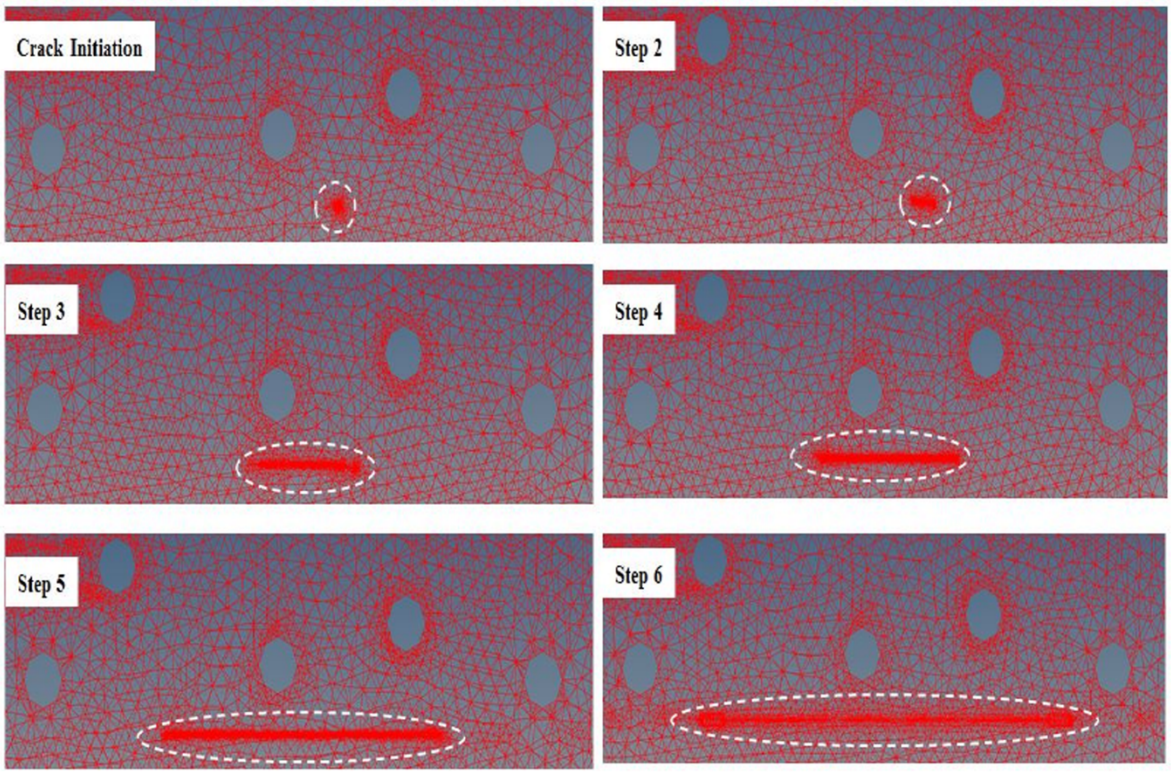

Fig. 9. Crack growth steps showing crack extension on frame under wireframe view.

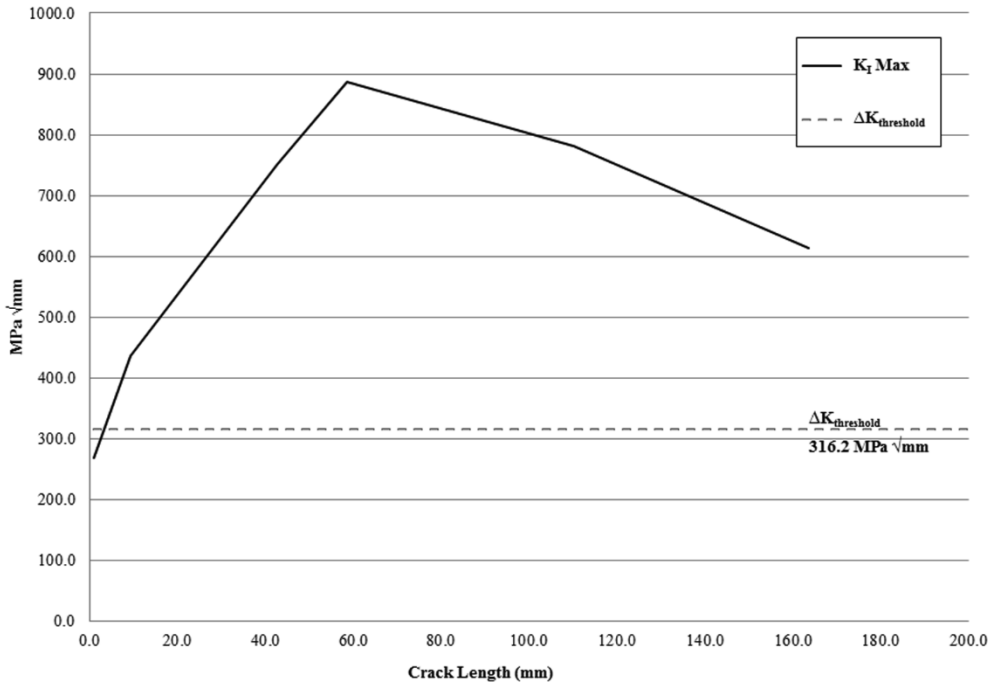

Fig. 10. Stress Intensity factors plotted against crack extension on frame.

crack in FRANC3D and using the NASTRAN solver for finite element analysis. In Fig. 10, maximum K_I, K_{II}, K_{III} obtained along crack fronts were plotted against crack length starting from the small initial semi-elliptical crack inserted at the location of high shear stress to the final crack growth step. This crack growth obtained under reverse bending loads in the lower flange of the frame was primarily Mode I dominated. This reverse bending causes high tensile stresses in inner surface and acts to open up any cracks present. Mode II and Mode III effects were present up to certain crack length and a small amount of crack kinking was seen along crack front. It was observed only when crack initiation exceeds certain size (~5 mm in crack length) a large fatigue crack growth was initiated.

Fig. 11(a) shows the deformed shape of the frame lower flange (scaled factor 10) under reverse bending loads and Fig. 11(b) shows the crack faces opening at step 6 during the crack growth progression. The crack initiated due to fretting fatigue grows under external loads when $\Delta K_I > \Delta K_{threshold}$ (Fracture toughness of heat treated high strength frame material was considered as 316.2 MPa √mm [16]).

4.1. Insertion of multiple cracks

It was observed in SEM micrographs, surface wear during fretting was spread along the lower edge contact of inner reinforcement

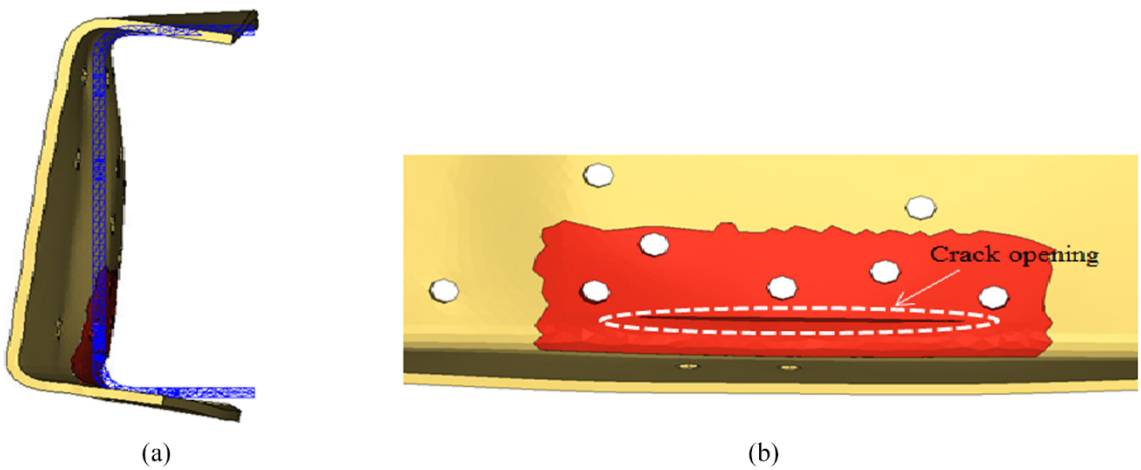

Fig. 11. (a) Reverse bending of frame flange (b) Crack opening under reverse bending–Step 6 result.

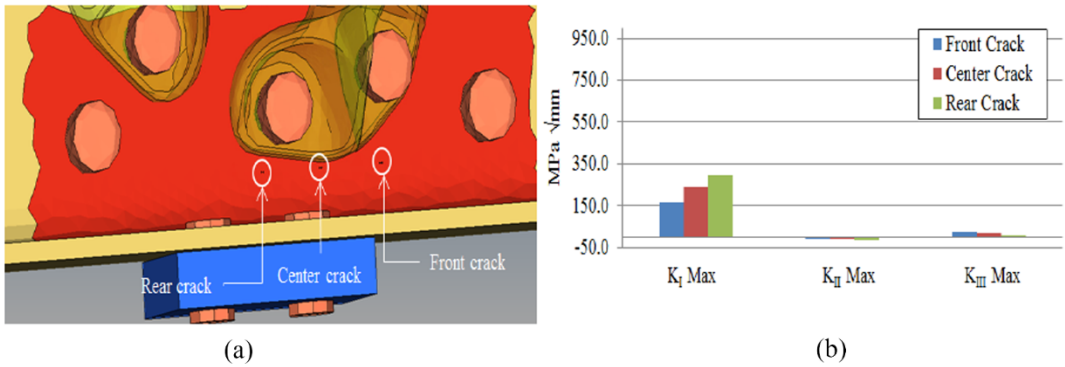

Fig. 12. (a) Multiple cracks initiated in fretting zone (b) Maximum stress intensity factors measured for initiated cracks.

plate to the frame section (Fig. 4). This would result in multiple crack initiation sites and during reverse bending loads these cracks must have coalesced to form the large longitudinal crack along the contact edge. The effect of multiple crack initiations was important to be understood since wear due to fretting will not result in one single surface defect. Fretting wear can result in deep surface pitting marks distributed along the contact area [5]. This was simulated by inserting three small semi-elliptical cracks (a = b = 0.5 mm) along the area of high fretting noticed in the optical micrographs. Fig. 12(a) shows small initial cracks (front, center and rear) each of them at an equal distance of 30 mm apart being inserted into local model, Fig. 12(b) shows maximum stress intensity factors obtained at crack tips. The distance between cracks was arbitrarily selected and the objective was to study the effect of multiple crack initiations and observe if multiple cracks coalesce and form a single large crack.

K_I was higher for rear crack which was located in area of high shear stress and bending moment under reverse bending loads. Although K_I was below $\Delta K_{threshold}$ for all three small initial cracks a larger initial semi-elliptical crack pushes stress intensity factors above threshold value and starts crack growth under fatigue. After several iterations the cracks grew large enough to coalesce forming a single large propagating crack. Fig. 13(a) shows crack paths connecting between the cracks after three steps of simulation and Fig. 13(b) shows stress intensity factors with larger K_I for rear crack which was under higher shear stress and bending moment.

5. Design solution to prevent fretting fatigue

It was observed from failure analysis that fretting fatigue occurred at the edge contact between the frame and the inner reinforcement plate in the area of the frame mid-section (lower bolt-hole location). This design was improved to reduce fretting wear by extending the inner reinforcement length a further 10 mm on the lower side as shown in Fig. 14. This adds more cross sectional area in order to distribute the contact driven shear stress. The reinforcing plate's lower edge was rounded resulting in cylindrical contact to further reduce the magnitude of the contact stress distribution.

Fig. 14(b) and (d) shows the optimal design obtained after 5 design iterations. In the baseline design of inner reinforcement, singular edge stresses along the inner edge contact were obtained. This sharp edge contact was modified to smoother rounded edge contact in the optimal solution. This profile change using a small radius (6 mm) eliminates local singularity due to sharp edge and provides smooth pressure distribution over the contact area.

Fig. 15(a) and (b) shows two blocks in contact under a normal load 'P' and with different contact edge conditions. The blocks are also subjected to relative displacement (sliding) under external loads and this results in shear stress distribution along the contact interface.

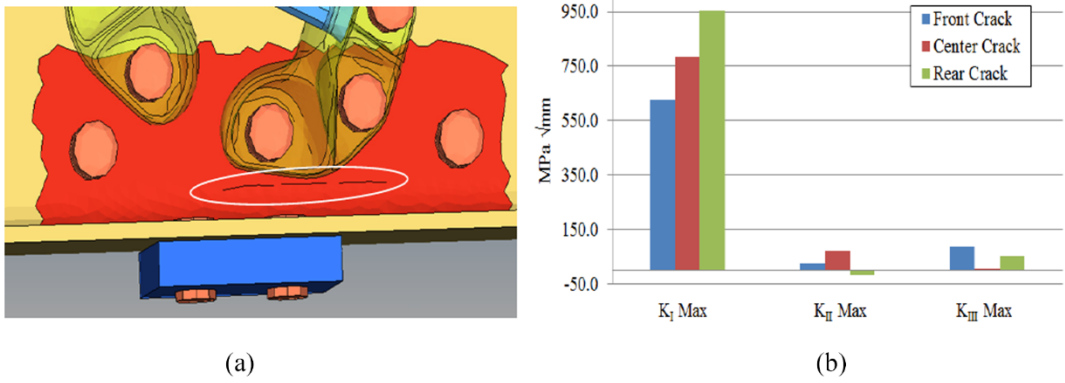

Fig. 13. (a) Crack growth obtained after 3 steps (b) Maximum stress intensity factors measured for cracks.

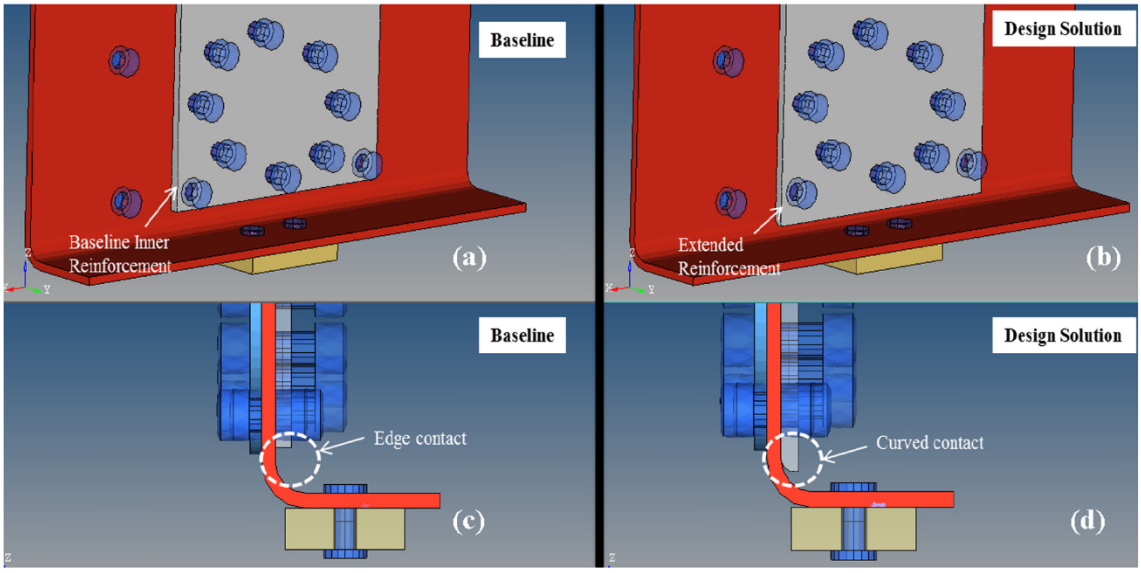

Fig. 14. (a) Baseline design of inner reinforcement (b) Design solution with extended inner reinforcement (c) Baseline side view showing edge contact (d) Design solution showing extended inner reinforcement with curvature added towards frame.

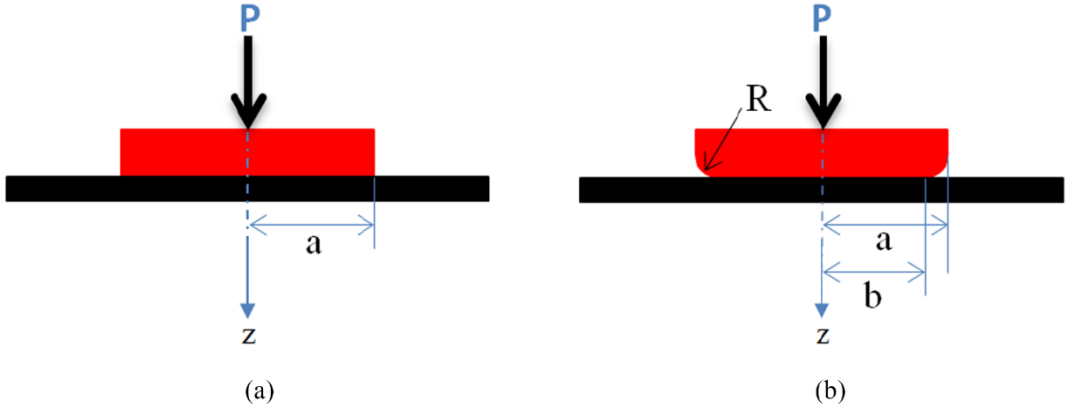

Fig. 15. Contact configurations (a) Flat ended with sharp edge contact (b) Flat ended with rounded edge contact.

The contact configuration in Fig. 15(a) was analogous to a rigid flat punch with sharp edge pressed in an elastic half-space problem and represents the contact condition of baseline design with inner reinforcement on frame (Fig. 14(c)). The contact configuration shown in Fig. 15(b) provides a smoother stress distribution and avoids edge singularity. This was analogous to the rigid flat punch with a rounded edge pressed in an elastic half-space problem and represents the contact condition of design optimal solution on frame (Fig. 14(d)).

Fig. 16 shows the pressure distribution for a flat indenter with rounded corners having varying (b/a = 0.0, 0.1,…,1) configurations [17]. The bold lines in the figure correspond to the limit cases with b/a = 0 indicating a circular contact and b/a = 1 for a flat edge contact. The half space is assumed to be homogeneous, isotropic, incompressible and linearly elastic [18].

Neglecting friction, contact normal stress distribution for a sharp edge contact (analogous to flat cylindrical rigid punch) is given as ([19,20]),

$$p(x) = \frac{P}{2\pi a\sqrt{a^2 - x^2}} \tag{6}$$

where *"x"* is horizontal axis, *"a"* is half width of block and *"P"* is the normal force. The normal stress approaches singularity at the edge location (when $\times \ = a$).

The analytical derivation of contact pressure distribution for Fig. 15(b) was given as [21],

$$p(x) = \frac{E}{2R(1-\nu^2)t}[(a^2 - x^2) - 2b(a - x)] \quad (b \le x \le a) \tag{7}$$

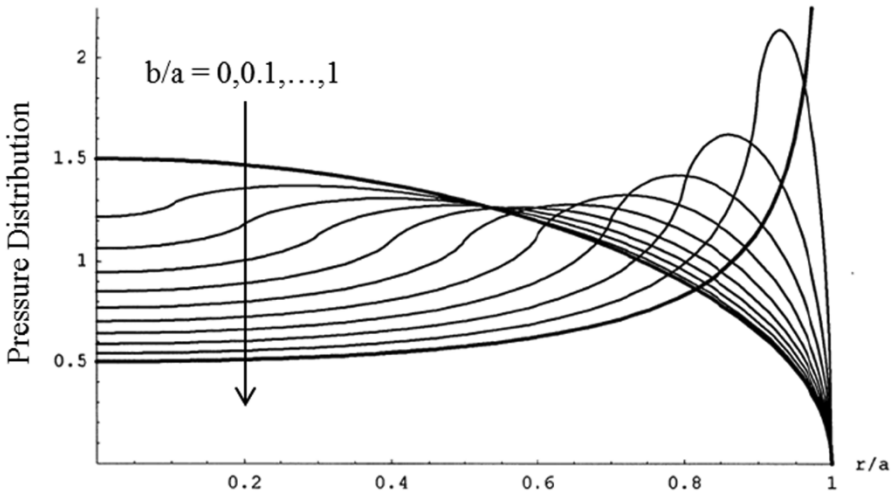

Fig. 16. Pressure distribution for a flat indenter with rounded corners (b/a = 0.0,0.1,…,1).

$$p(x) = \frac{E}{2R(1-\nu^2)t}(a-b)^2 \quad (0 \le x \le b) \tag{8}$$

where *"E"* is material elastic modulus, *"ν"* is poisson's ratio, *R* is the edge radius, *"t"* is plate thickness and *"b"* is the contact half width.

The contact stress distribution for rounded edge condition can be considered using a function of Muskhelisvili potential, as was discussed by Jager [20] and Ciavarella et al. [22]. The final design optimal solution was based on the above fundamental analytical reasoning.

The optimal design selected was compared to baseline design for all critical load events, Fig. 17 shows shear stress plot for frame articulation on both baseline and final design solution. The optimal design solution provides a large reduction in stress magnitude along the fretting zone. In Fig. 18(a) fatigue damage plot on frame for baseline design indicates high damage in the area of fretting zone, a damage of "0.733" was obtained. A comparative fatigue damage plot for the design optimal solution is shown in Fig. 18(b). There was a large reduction in fatigue damage for the optimal solution, with maximum damage in the fretting zone reducing from "0.733" to "0.0572". These calculations indicate that fatigue damage is significantly reduced with the optimal design and if implemented should significantly reduce the risk of fretting-fatigue cracking at this location given the same testing regime.

6. Conclusions

The paper was primarily focused on fretting fatigue crack growth on frame rail of a heavy duty truck. The 3D crack growth simulation program FRANC3D was combined with finite element analysis results (NASTRAN) to determine stress intensity factors, crack orientation and number of cycles to grow the crack. The fretting fatigue crack growth of frame rail was simulated using full

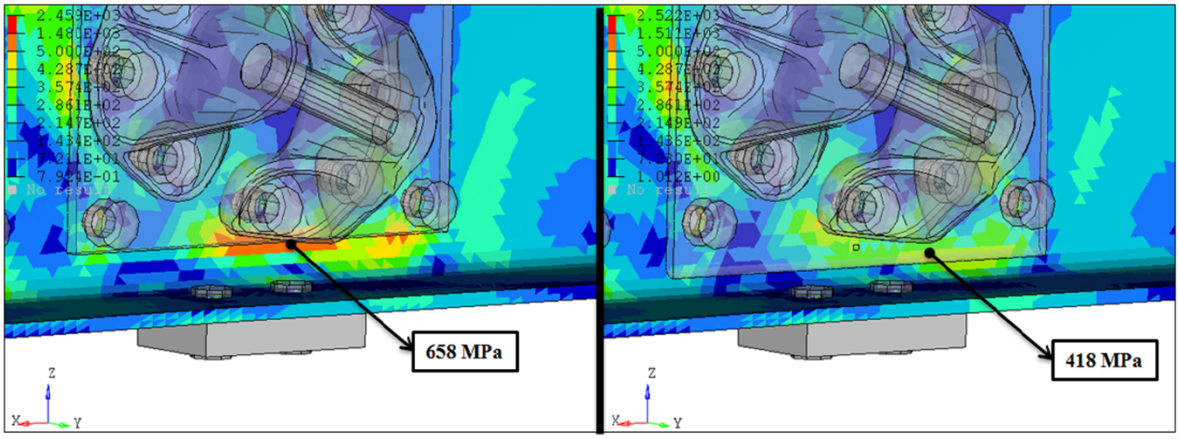

Fig. 17. Comparison of shear stress plot for frame articulation event (a) Baseline design (b) Optimal design with extended inner reinforcement.

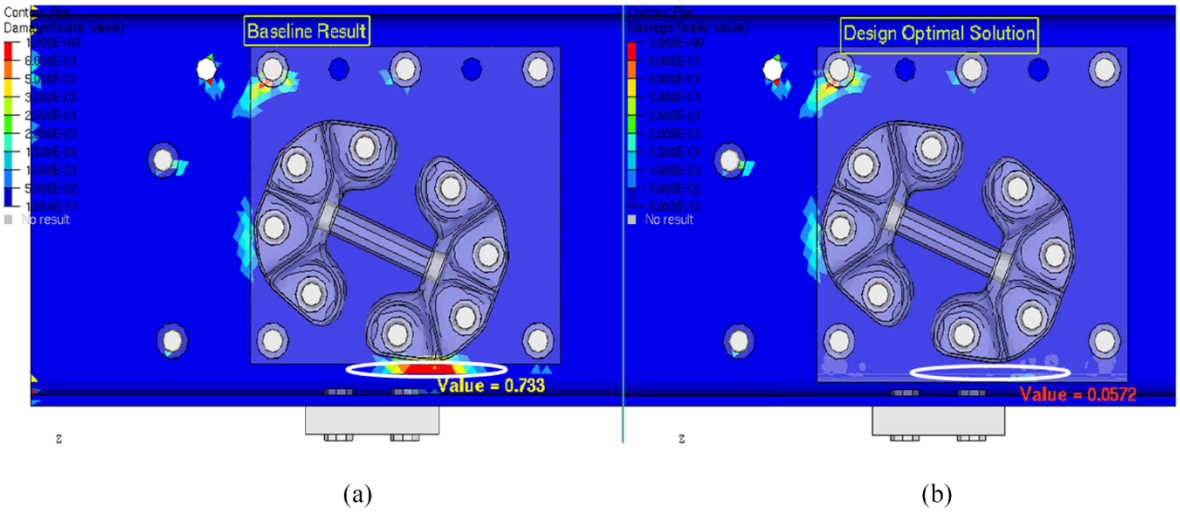

Fig. 18. Comparison of fatigue damage plot (a) Baseline design with high damage in fretting zone (b) Optimal design solution with large improvement in fatigue life.

vehicle dynamic response of a heavy duty truck derived from accelerated endurance test of the vehicle. The following conclusions were drawn from this work:

- Visual inspection and metallographic study of frame fatigue failure indicated that the crack initiation occurred in a region of fretting wear and the crack grew under reverse bending loads on frame rail.
- The crack kink angle was determined using strain energy release rate method and "Paris law" was used for fatigue growth rate model. The stress intensity factors were computed using Interaction Integral (M-Integral) method and included the effects of crack face contact. Mode I stress intensity factor was found to be dominant during reverse bending fatigue of frame.
- The simulation results obtained for frame fretting fatigue using loads determined from vehicle endurance testing properly predicted the location of crack initiation as well as the crack path. The maximum fatigue damage predicted through simulation in the fretting zone indicated a potential failure during full vehicle endurance test.
- The effect of multiple crack initiations due to fretting wear was studied by inserting multiple cracks in the fretting zone. It was observed that the cracks would coalesce during growth and result in a large crack as obtained during full vehicle endurance test.
- An optimal design solution was identified to reduce fretting induced shear stresses. This involved changing the contact configuration of the inner reinforcement from a sharp edge contact to a rounded edge contact. Adding rounded corners for the reinforcement plate helps avoid stress concentration in the fretting zone. The length of inner reinforcement lower edge was increased by additional 10 mm to add more cross-sectional area in distribution of contact stresses.

Acknowledgement

The research presented here was partially carried out at the Advanced Calculations group of Chassis Vehicle Dynamics and Engineering (CVDE) section of Volvo Group North America, Greensboro, North Carolina, USA. The authors would like to thank Dr. Omar Ibrahim at Process Optimization Corporation for providing support and license for FRANC3D program in this research.

References

[1] J.M. Dobromirski, Variables of Fretting Process: Are There 50 of Them? Standardization of Fretting Fatigue Test Methods" and Equipment, ASTM STP 1159, 1992, pp. 60–66.
[2] G.H. Majzoobi, R. Hojjati, M. Soori, Fretting fatigue behavior of Al7075-T6 at sub-zero temperature, Tribology Int. 44 (11) (2011) 1443–1451, https://doi.org/10.1016/j.triboint.2011.03.021.
[3] D.A. Hills, D. Nowell, Mechanics of fretting fatigue, Kluwer Academic Publishers, 1994.
[4] T.L. Anderson, Mechanics: fundamentals and applications, Third Ed., CRC Press, 2005 June 24.
[5] R. Hojjati Talemi, M. Abdel Wahab, P. De Baets, Numerical modelling of fretting fatigue, J. Phys. 305 (2011).
[6] B.J. Carter, E.C. Schenck, P.A. Wawrzynek, A.R. Ingraffea, K.W. Barlow, Three-dimensional simulation of fretting crack nucleation and growth, Eng. Fract. Mech. 96 (2012) 447–460.
[7] K.W. Barlow, R. Chandra, Fatigue crack propagation simulation in an aircraft engine fan blade attachment, Int. J. Fatigue 27 (2005) 1661–1668.
[8] R. Rajasekaran, D. Nowell, Fretting fatigue in dovetail blade roots: Experiment and analysis, Tribol. Int. 39 (2006) 1277–1285.
[9] A. Mechanics, T. Ferjaoui, M. Abdel Yue, R. Hojjati-Talemi Wahab, Prediction of fretting fatigue crack initiation in double lap bolted joint using Continuum Damage, Int. J. Fatigue 73 (2015) 66–76.
[10] O. Jin, S. Mall Wear, Effects of slip on fretting behavior: experiments and analyses, Wear 256 (2004) 671–684.
[11] H. Proudhon, S. Basseville, Finite element analysis of fretting crack propagation, Eng. Fract. Mech. 78 (2011) 685–694.
[12] E. Giner, C. Navarro, M. Sabsabi, M. Tur, J. Domınguez, F.J. Fuenmayor, Fretting fatigue life prediction using the extended finite element method, Int. J. Mech. Sci. 53 (2011) 217–225.

[13] E. Giner, Mohamad Sabsabi, Juan Jose Rodenas, F. Javier Fuenmayor, Direction of crack propagation in a complete contact fretting-fatigue problem, Int. J. Fatigue 58 (2014) 172–180.
[14] Prithvi Raj Arora, M.S.D. Jacob, Mohd.Sapuan Salit, Elsadig Mahdi Ahmed, M. Saleem, Prasetyo Edi, Experimental evaluation of fretting fatigue test apparatus, Int. J. Fatigue 29 (2007) 941–952.
[15] A.W. Aditya, D.L. Benjamin, Farshid Sadeghi, Behrooz Jalalahmadi, Nathan Bolander, An experimental study and fatigue damage model for fretting fatigue, Tribol. Int. 79 (2014) 183–196.
[16] S. Fleming, Fatigue crack growth for typical CV siderail hole-making processes applied to heat-treated steel (MET1123) and ultra-high strength low alloy steel (120XF), SAE International, 2009, https://doi.org/10.4271/2009-01-2863.
[17] Michele Ciavarella, Indentation by nominally flat or conical indenters with rounded corners, Int. J. Solids Struct. 36 (1999) 4149–4181.
[18] V.R. Krishnan, C.-Y. Hui, Large deformation of soft elastic materials in adhesive contact with a rigid cylindrical flat punch, Soft Matter 4 (2008) 1909–1915.
[19] Alexander Konyukhov, Ridvan Izi, Introduction to computational contact mechanics, John Wiley and Sons Ltd., 2015.
[20] J. Jager, New analytical and numerical results for two-dimensional contact profiles, Int. J. Solids Struct. 39 (2002) 959–972.
[21] M.J. Jaffar, Frictionless contact between an elastic layer on a rigid base and a circular at-ended punch with rounded edge or a conical punch with rounded tip, Int. J. Mech. Sci. 44 (2002) 545–560.
[22] G. Macinab, M. Ciavarella, New results for the fretting-induced stress concentration on Hertzian and flat rounded contacts, Int. J. Mech. Sci. 45 (2003) 449–467.
[23] Vinay N Rao, Development of Simulation Methodology to Predict Crack Growth Behavior in Heavy Duty Truck Components using Full Vehicle Response Dynamic Loads, PhD Dissertation, NC State 2016.